RSC Advances

PAPER

View Article Online
View Journal | View Issue

Cite this: *RSC Adv.*, 2021, **11**, 27309

Zn^{2+} removal from the aqueous environment using a polydopamine/hydroxyapatite/Fe_3O_4 magnetic composite under ultrasonic waves†

Rauf Foroutan,[a] Seyed Jamaleddin Peighambardoust,[a] Saeed Hemmati,[b] Amir Ahmadi,[b] Ermelinda Falletta,[de] Bahman Ramavandi*[c] and Claudia L. Bianchi*[de]

Received 13th June 2021
Accepted 3rd August 2021

DOI: 10.1039/d1ra04583k

rsc.li/rsc-advances

In this study, an easily magnetically recoverable polydopamine (PDA)-modified hydroxyapatite (HAp)/Fe_3O_4 magnetic composite (HAp/Fe_3O_4/PDA) was suitably synthesized to exploit its adsorption capacity to remove Zn^{2+} from aqueous solution, and its structural properties were thoroughly examined using different analytical techniques. The effect of multiple parameters like pH, ultrasonic power, ultrasonic time, adsorbent dose, and initial Zn^{2+} concentration on the adsorption efficiency was assessed using RSM-CCD. According to the acquired results, by increasing the adsorbent quantity, ultrasonic power, ultrasonic time, and pH, the Zn^{2+} adsorption efficiency increased and the interaction between the variables of ultrasonic power/Zn^{2+} concentration, pH/Zn^{2+} concentration, pH/absorbent dose, and ultrasonic time/adsorbent dose has a vital role in the Zn^{2+} adsorption. The uptake process of Zn^{2+} onto PDA/HAp/Fe_3O_4 followed Freundlich and pseudo-second order kinetic models. The maximum capacity of Zn^{2+} adsorption (q_m) obtained by PDA/HAp/Fe_3O_4, HAp/Fe_3O_4, and HAp was determined as 46.37 mg g^{-1}, 40.07 mg g^{-1}, and 37.57 mg g^{-1}, respectively. Due to its good performance and recoverability (ten times), the HAp/Fe_3O_4/PDA magnetic composite can be proposed as a good candidate to eliminate Zn^{2+} ions from a water solution.

Introduction

The economic development and the rapid growth of agricultural industries have primarily contributed to the production of wastewater containing organic and inorganic pollutants, which when discharged into the environment can cause serious problems for human health, water resources, and other living organisms.[1–3] Among the organic and inorganic pollutants, dyes, drugs, and heavy metals have received paramount attention due to their high environmental persistence and toxicity.[3,4] Recently, the removal of heavy metals from water matrices has become an important concern and research topic because of the strong impact that this class of pollutants has on human health, and the environment.[5] Heavy metals find application in various industrial sectors, such as the metal plating, electroplating, mining, leather, and fertilizer industries, and, as a consequence, every year directly or indirectly a large number of these pollutants, mainly zinc, copper, nickel, arsenic, lead, cadmium, chromium, mercury, and cobalt, enter the environment through industrial wastewater discharge.[6–8] It has been demonstrated that toxic metals can enter the human body through food chains and their accumulation has been linked to the onset of various diseases and illnesses such as neurological disorders, various cancers, imbalances in hormones, obesity, abortion, asthma, infertility, and death.[9] The zinc ion is one of the most employed metals in the industrial field. Even though it is an important and essential micronutrient for life, in high concentrations it can lead to depression, lethargy, increased thirst, neurological disorders, diarrhoea, anaemia, kidney failure, and low immunity.[10,11] Owing to its hazardous nature for public health, the maximum Zn concentration in seawater is 40 μg L^{-1} and in freshwater is 45–500 μg L^{-1}, strongly correlated to the water hardness.[12] Therefore, it is evident that improper discharge of toxic metal ions into the water bodies is an important issue and their removal from aqueous systems before releasing them to the environment is crucial.

[a]*Faculty of Chemical and Petroleum Engineering, University of Tabriz, Tabriz, 5166616471, Iran*

[b]*Department of Chemical Engineering, Bushehr Branch, Islamic Azad University, Bushehr, Iran*

[c]*Departments of Environmental Health Engineering, Faculty of Health and Nutrition, Bushehr University of Medical Sciences, Bushehr, Iran. E-mail: b.ramavandi@bpums.ac.ir*

[d]*Università degli Studi di Milano – Department of Chemistry,* via *Golgi 19, 20133 Milan, Italy. E-mail: claudia.bianchi@unimi.it*

[e]*Consorzio Interuniversitario Nazionale per la Scienza e Tecnologia dei Materiali (INSTM),* via *Giusti 9, 50121 Florence, Italy*

† Electronic supplementary information (ESI) available. See DOI: 10.1039/d1ra04583k

So far, various techniques like electrochemical methods, coagulation, ion exchange, chemical precipitation, membrane filtration, biological treatment, and adsorption have been used to eliminate metals from wastewaters.[13,14] Most of these approaches show drawbacks, such as high operating costs, sensitive operating status, low efficiency, and secondary sludge production,[15] which has limited their use on an industrial scale. In particular, if compared to the other processes, the adsorption method is an effective way for pollutants abatement from wastewater,[16] thanks to its simplicity, low cost, high performance and efficiency, low selectivity, and no production of secondary sludge.[17–19] In addition to the mentioned advantages, when the content of metal ions in industrial wastewater is in the range of 10–100 mg L^{-1} or the concentration of ions of discharged metals is less than 1 mg L^{-1}, the adsorption method is effective.[3]

In the last years for this kind of application, various solid sorbents have been investigated, such as *Tamarix hispida* activated carbon,[20] *Aspergillus flavus* biomass,[21] magnetic $MnFe_2O_4$,[22] and nano bentonite.[23] Among them, due to its unique properties, such as low cost, insolubility in water ($K_{ps} \approx 10^{-59}$), the high adsorption capacity of heavy metals, availability, suitable thermal and chemical stability, calcium hydroxyapatite (HAp) has been the main focus of numerous studies.[24,25] Thanks to the presence of calcium, hydroxyl, and phosphate ions in the crystalline structure, it can effectively sorb heavy metals through ion exchange or electrostatic interactions.[26] Although HAp has exhibited evident and significant advantages, its constituent particles are prone to aggregation and clump formation, causing a decrease in their active surface and dispersion in aqueous media and finally reducing their performance towards pollutants removal.[27] Moreover, HAp is characterized by poor mechanical and high abrasive properties that can be improved by combining this material with synthetic polymers, biopolymers, and nanoparticles. HAp increases crystallization, morphology, dimensional anisotropy and improves the adsorption capacity of the composite.[28] In addition to HAp, polydopamine (PDA) is another interesting material that has recently attracted the attention of the scientific community in particular in the field of nanotechnology, materials chemistry, and medicine and has been used in lithium-ion batteries, tissue engineering, bioimaging, biosensors, *etc*.[29,30] PDA is very sticky and belongs to the category of catecholamines, which has a benzene ring in its structure and functional groups such as amines, imines, and phenols, which make this polymer function properly in removing heavy metals through electrostatic interactions.[31] Adding iron-containing compounds like Fe_3O_4 to adsorbents can create magnetic properties and use less force to separate them from the refined solution.[32]

In the present study, we propose an innovative PDA/HAp/Fe_3O_4 magnetic composite based on hydroxyapatite produced in our laboratory from a biological source (chicken bone) characterized by outstanding ability to remove Zn^{2+} ions from an aqueous solution. HAp/Fe_3O_4/PDA was extensively characterized by various techniques. To assess the influence of the reaction parameters in the adsorption process, like pH, temperature, time, Zn^{2+} ions concentration, and adsorbent mass, the Response Surface Method-Central Composite Design (RSM-CCD) was used. Different models were utilized to explore the equilibrium, kinetic and thermodynamic behaviour of the adsorption process and the type of process was examined physically, chemically, spontaneously, or non-spontaneously. Finally, the effect of co-existing ions and phenomena of adsorption/desorption were also investigated.

Experimental section

Chemicals and materials

Iron(II) chloride tetrahydride ($FeCl_2 \cdot 4H_2O$), iron(III) chloride hexahydride ($FeCl_3 \cdot 6H_2O$), HCl, NaOH, ethanol, zinc nitrate tetrahydride ($Zn(NO_3)_2 \cdot 4H_2O$), and dopamine hydrochloride was purchased from Merck Co. with high purity. To prepare the initial solutions for the Zn^{2+} adsorption process, the stock solution was diluted using distilled water. To regulate the pH of the desired aqueous solutions, NaOH and HCl solutions (0.1–1 M) were added dropwise. Chicken bones were obtained from local restaurants and used as a primary source for the production of hydroxyapatite.

Synthesis of PDA/HAp/Fe_3O_4 composite

HAp production was prepared using the calcination process and chicken bones as a suitable primary source according to the previously described method.[33] 50 g of the chicken bones were washed with distilled water and dried for 24 h at 105 °C. The dried bones were first exposed to a direct flame to become fully carbonized and then, the carbonized bones were calcinated at 1000 °C for 4 h. The change in color of the bones from black to white indicates HAp formation. This latter was powdered using a ball mill for 24 h and granulated using sieve no. 25 (ASTM E11) and then stored at room temperature.

The HAp/Fe_3O_4 magnetic composite was synthesized using a co-precipitation method previously described.[34] To modify HAp/Fe_3O_4 magnetic composite by polydopamine coating, 1 g of HAp/Fe_3O_4 magnetic composite was added to 100 mL of distilled water at pH 8.5 and subjected to an ultrasonic wave for 30 min. At the end of this time, 0.7 g of dopamine hydrochloride was added and stored at room temperature for 24 h under stirring. The PDA-modified composite particles were isolated from the aqueous solution using a magnet and washed several times using distilled water, and ethanol and then dried for 24 h at 50 °C. The synthesized composite was powdered using a ball mill and stored at ambient temperature.

Batch adsorption study using RSM-CCD

The interactions and effects of influential parameters on the Zn^{2+} ions adsorption by PDA/HAp/Fe_3O_4 magnetic composite were studied in batch mode in the presence of ultrasonic process (35 kHz) using RSM-CCD methodology. The effect of independent parameters, like pH (2–6), ultrasonic power (100–300 W), Zn^{2+} ions (10–30 mg L^{-1}), composite dose (0.4–1.2 g L^{-1}), and time (10–50 min) was investigated at five levels ($-\alpha$, -1, 0, 1, $+\alpha$). Table 1 shows more details for the independent

parameters. Based on the number of parameters (n) and their levels, the experiments number was included $2^n + 2n + 4 = 46$, where the number 4 is the repetitions number in the central points. An acetylene–air fuel flame atomic absorption spectrometer (Varian AA240FS) was used to measure the concentration of Zn^{2+} ions remaining in the aqueous solution. During the adsorption tests, the adsorption percentages (R%) of Zn^{2+} ions and elimination capacity (q_e) were determined from eqn (1) and (2), respectively:

$$R\ (\%) = \left(\frac{C_i - C_e}{C_i}\right) \times 100 \quad (1)$$

$$q_e = (C_i - C_e)\frac{V}{m} \quad (2)$$

Here C_i and C_e (mg L^{-1}) denote the initial and equilibrium contents of Zn^{2+} ions, V reflects the volume of used solution (L), and m denotes the sorbent weight (g).

To analyze the obtained experimental data based on the suggestion of Design-Expert software, a 2-degree polynomial model was applied. This polynomial model shows the link between the independent variables (X_1 to X_5) and the dependent variable (Y) as described by eqn (3):

$$Y = \beta_0 + \sum_{i=1}^{5}\beta_i X_i + \sum_{i=1}^{5}\sum_{j=1}^{5}\beta_{ij}X_iX_j + \sum_{i=1}^{5}\beta_{ii}X_i^2 + \varepsilon \quad (3)$$

Here, Y implies the desired response, β_0 implies the model constant-coefficient, β_i implies the linear coefficients, β_{ij} implies the interaction coefficients, β_{ii} implies the quadratic coefficients, ε reflects the residual time, and X_i and X_j are the independent variables that are known in each laboratory step. The obtained data were processed using Design-Expert 11.0 software and the analysis of variance (ANOVA) was examined to acquire the link between the process and response variables. The authenticity of the polynomial model was determined by assessing the correlation coefficient (R^2) and its statistical significance by the value of the F-test.

Desorption studies

For the desorption studies, 1.2 g L^{-1} of PDA/HAp/Fe_3O_4 magnetic composite, HAp/Fe_3O_4 magnetic composite, and HAp were added to aqueous solutions containing Zn^{2+} ion (10 mg L^{-1}) in optimal laboratory conditions, and an ultrasonic process was performed. After the adsorption experiments, Zn^{2+} ions remaining in the aqueous solution, as well as the percentage of adsorbed Zn^{2+} ions were determined by atomic absorption spectroscopy, as reported above. Then, each adsorbent was put in 50 mL of 0.75 M HCl solution and magnetically stirred for 2 h. Finally, the adsorbents were removed from the reaction media and the metal content of the solutions was determined. Each material was regenerated and reused 10 stages and its adsorption/desorption ability was investigated.

Materials characterization

The structure of the HAp and magnetic composites was characterized by a FT-IR spectroscopy (PerkinElmer system 2000). In the case of PDA/HAp/Fe_3O_4 magnetic composite, the FT-IR analysis was carried out pre- and post- zinc adsorption X-ray diffraction analyses were carried out by a D8 Focus diffractometer (Bruker Corporation, Germany) working with Cu Kα radiation (1.5405 Å) and at 40 kV × 20 mA nominal X-ray power. Porosity and surface area analyses were measured according BET method (ASAP 2460, Micromeritics Corporation, United States). For X-ray photoelectron spectroscopy (XPS) analyses a K-alpha 1063XPS apparatus (Thermo Fisher Scientific, USA) was used. The magnetic behavior of the samples was analyzed by a vibrating sample magnetometer (Lakeshore, model 7410). The micro-structure, adsorbent size, and surface morphology were characterized by scanning electron microscope (SEM, REGULUS8230, Hitachi, Japan) and transmission electron microscope (TEM, HT7700, Hitachi, Japan). Atomic force microscopy (AFM, Dimension Icon) was applied to evaluate the surface roughness of adsorbents samples.

Results and discussion

Characterization of adsorbents and composites

Fig. 1a depicts the FT-IR spectra of HAp from chicken bones, HAp/Fe_3O_4, and HAp/Fe_3O_4/PDA magnetic composites were investigated before and after Zn^{2+} ions removal. Concerning the FT-IR spectra of the materials before the metal adsorption, in the HAp spectrum, the wavenumbers at 1046 cm^{-} and 566 cm^{-1} respectively can be linked to the asymmetric vibrations of P–O and O–P–O.[35] Moreover the band at 1695 cm^{-1} and that at 1462 cm^{-1} are due to the presence of –OH and C–O functional groups, as previously reported.[36] After modification of HAp by Fe_3O_4 nanoparticles (HAp/Fe_3O_4), the previously described bands showed a slight shift because of the interactions between Fe_3O_4 nanoparticles and functional groups of the HAp structure. For example, for HAp/Fe_3O_4 composite the vibration of

Table 1 The variables and coding levels

			Factorial and center level			Axial level	
Independent variables	Coded	Unit	Low (−1)	Center (0)	High (+1)	Lowest (−α)	Highest (+α)
Power of ultrasound	X_1	°C	150	200	250	100	300
pH	X_2	—	3	4	5	2	6
Content Zn^{2+}	X_3	mg L^{-1}	15	20	25	10	30
Sonication time	X_4	min	20	30	40	10	50
Adsorbent dosage	X_5	g L^{-1}	0.6	0.8	1	0.4	1.2

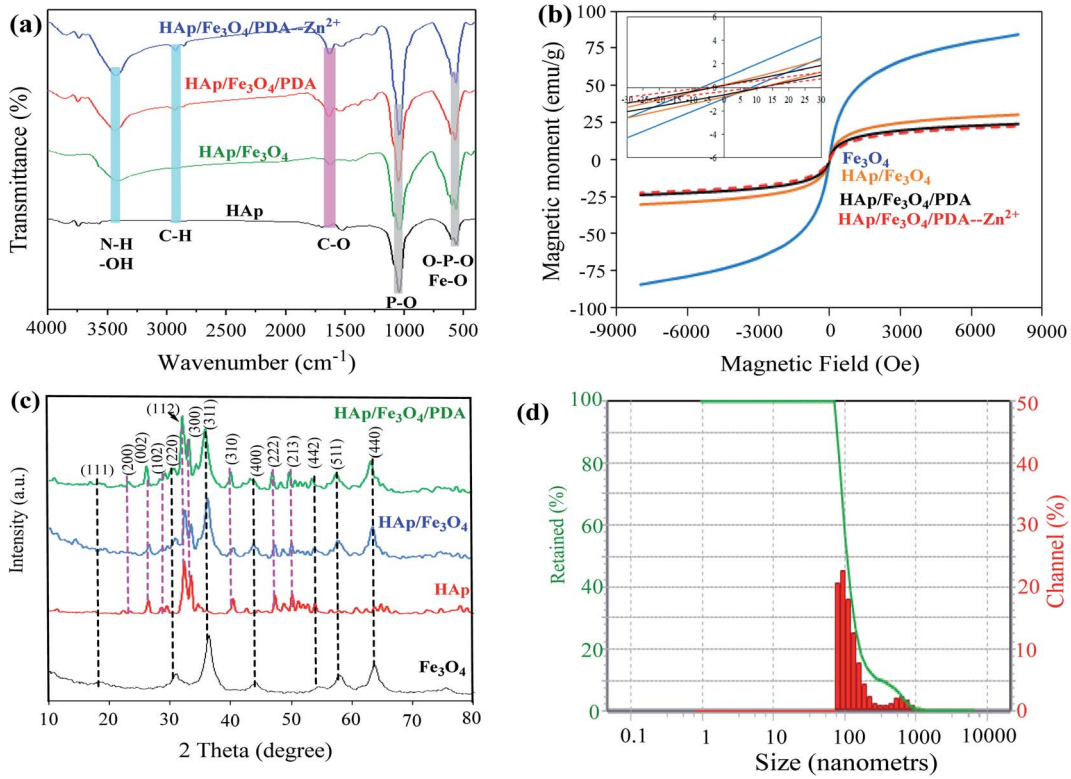

Fig. 1 (a) FT-IR and (b) VSM images of HAp, HAp/Fe_3O_4 and PDA/HAp/Fe_3O_4/magnetic composites before and after Zn^{2+} adsorption process, (c) XRD patterns of all the samples, and (d) DLS graphic of PDA/HAp/Fe_3O_4 magnetic composite.

566 cm^{-1} in the HAp structure moved to 567 cm^{-1}, indicating the interaction of the O–P–O functional group with Fe_3O_4 nanoparticles. It is worth noting that the typical absorption peak of Fe_3O_4 at 570 cm^{-1}[34] overlaps with the O–P–O vibration band. In the FT-IR spectrum of PDA/HAp/Fe_3O_4 magnetic composite, additional low-intensity peaks appeared in the span of 1400–1510 cm^{-1}, which are due to C–C and C–N vibrations in the PDA structure.[37] Moreover, C–H vibrations can be responsible for the low-vibration peak observed at 2922 cm^{-1}. After the Zn^{2+} ions adsorption process, the vibration intensity linked to PDA/HAp/Fe_3O_4 functional groups changed, probably because of the interactions with the zinc ions. The change in the vibrations intensity of and the position of the functional groups in HAp/Fe_3O_4/PDA after the adsorption was not very extensive, which shows that the adsorption of zinc ions using the desired composite is physically.

To magnetically separate and reuse the adsorbents, they must have the appropriate magnetic properties.[38] For this aim, the magnetic properties of Fe_3O_4, HAp/Fe_3O_4, and PDA/HAp/Fe_3O_4 magnetic composites were investigated pre- and post-Zn^{2+} adsorption. The results are reported in Fig. 1b. The value of magnetic saturation (M_s) for Fe_3O_4, HAp/Fe_3O_4, and PDA/HAp/Fe_3O_4 magnetic composites pre- and post- Zn^{2+} adsorption was determined as 84.283 emu g^{-1}, 30.305 emu g^{-1}, 24.014 emu g^{-1}, and 22.571 emu g^{-1}, respectively. The diminish in the level of magnetic saturation in the HAp/Fe_3O_4 and PDA/HAp/Fe_3O_4 samples can be due to the decrease in the amount of magnetic material, the non-magnetic nature of the matrix material, and the composite coating.[4] The presence of non-magnetic particles such as HAp and PDA in the structure of Fe_3O_4 reduces the magnetic torque.[39] As a result, the amount of magnetic saturation decreases, confirming the qualitative composition of HAp/Fe_3O_4 and PDA/HAp/Fe_3O_4. Although the magnetic saturation of both HAp/Fe_3O_4 and PDA/HAp/Fe_3O_4 magnetic composites decreased in comparison to Fe_3O_4, it is sufficient for magnetic separation from aqueous solutions. In addition, these materials show paramagnetic behavior due to negligible coercivity (H_c) and remanent magnetization (M_r).[40] Therefore, they can be easily isolated from liquid medium using a magnetic field (magnet) and reused.

The XRD patterns of HAp/Fe_3O_4, Fe_3O_4, and PDA/HAp/Fe_3O_4 magnetic composites allowed to investigate the structural properties of these materials, and the results are illustrated in Fig. 1c. For the Fe_3O_4 magnetic sample, peaks at a diffraction angle of 18.28, 30.14, 35.43, 43.1, 53.47, 56.98, and 63.04 2θ (°) were observed, which correspond to the crystal plates of (111), (220), (311), (400), (442), (511) and (440) respectively in pure Fe_3O_4 nanoparticles with inverted spinel structure according to the JCPDS card number 19-0629.[41] Besides, peaks in the diffraction angle range of 2θ equal to 10–80° were observed in the HAp structure, which represents different crystal plates in the HAp structure (ICDD file no. 01-079-8093).[42] The produced HAp had a hexagonal structure.[43,44] After modification of HAp by Fe_3O_4 and PDA, new vibrations related to Fe_3O_4 and HAp crystalline plates have been successfully observed in the structure of the samples, which shows that the inverted spinel structure of Fe_3O_4 and the hexagonal HAp had a good interaction, and have been successfully incorporated into the composites structure.

The DLS analyses were performed to determine the particle size of PDA/HAp/Fe_3O_4 and the acquired finding are depicted in Fig. 1d. 90.1% and 9.9% of PDA/HAp/Fe_3O_4 magnetic nanocomposite have a particle size of 103.8 nm and 610 nm respectively and the polydispersity index (PDI) was 14.78.

N_2 physical adsorption tests were performed to calculate specific surface area, pore-volume, and pore diameter of Fe_3O_4, HAp/Fe_3O_4, and PDA/HAp/Fe_3O_4 magnetic composites (Fig. 2). N_2 adsorption–desorption isotherms for all the three samples followed the type IV isotherms and had a residual ring at a relative pressure of P/P_0 in the range of 0.5–1, which shows monolayer adsorption[45] and the produced materials are mesoporous.[46] As the pore diameter is in the range of 2–50 nm all three types of materials have a mesoporous structure according to the IUPAC standard.[47] The specific active surface for Fe_3O_4, HAp/Fe_3O_4, and PDA/HAp/Fe_3O_4 magnetic composites was computed to be 72.148 $m^2\ g^{-1}$, 53.294 $m^2\ g^{-1}$, and 37.536 $m^2\ g^{-1}$ respectively. As the results show, specific areas of HAp/Fe_3O_4 and PDA/HAp/Fe_3O_4 are lower than Fe_3O_4 nanoparticles, which can be due to coverage of some pores and cavities in by PDA and Fe_3O_4 nanoparticles. It should also be noted that with the addition of HAp and PDA in the structure, the pore volume of Fe_3O_4 was reduced, which confirms the good placement and interaction between the components.

SEM and Map-EDX methods were used to investigate the morphology and interaction between HAp, Fe_3O_4, and PDA in the composites structure (Fig. S1†). The results showed that HAp synthesized from chicken bones has a hexagonal morphology with a Ca/P w/w ratio of 0.95 (Fig. S1a–c†). After the modification of HAp by Fe_3O_4, different sizes particles (spherical morphology) appeared on the surface of HAp, related to the presence of magnetic particles (Fig. S1d†), as confirmed by Map-EDX (Fig. S1e and f†). After coating the surface of HAp/Fe_3O_4 magnetic composite with PDA, the density and accumulation of particles on the composite surface increased, which could be due to the coating of PDA on HAp/Fe_3O_4 magnetic composite (Fig. S1g†). Map-EDX test was carried out to confirm the presence of PDA on the surface of HAp/Fe_3O_4 magnetic composite, which showed the presence of N and C elements (Fig. S1h and i†). The observation of N and C elements in the composite structure confirms the existence of PDA in the composite structure and, as a consequence, that the PDA/HAp/Fe_3O_4 magnetic composite has been successfully synthesized.

Two-dimensional and three-dimensional analyzes by AFM and TEM techniques were carried out to deepen the study on morphology and structure, of these materials. The AFM images (Fig. S2a†) showed that after the addition of Fe_3O_4 nanoparticles and PDA in the structure of HAp, and the formation of the

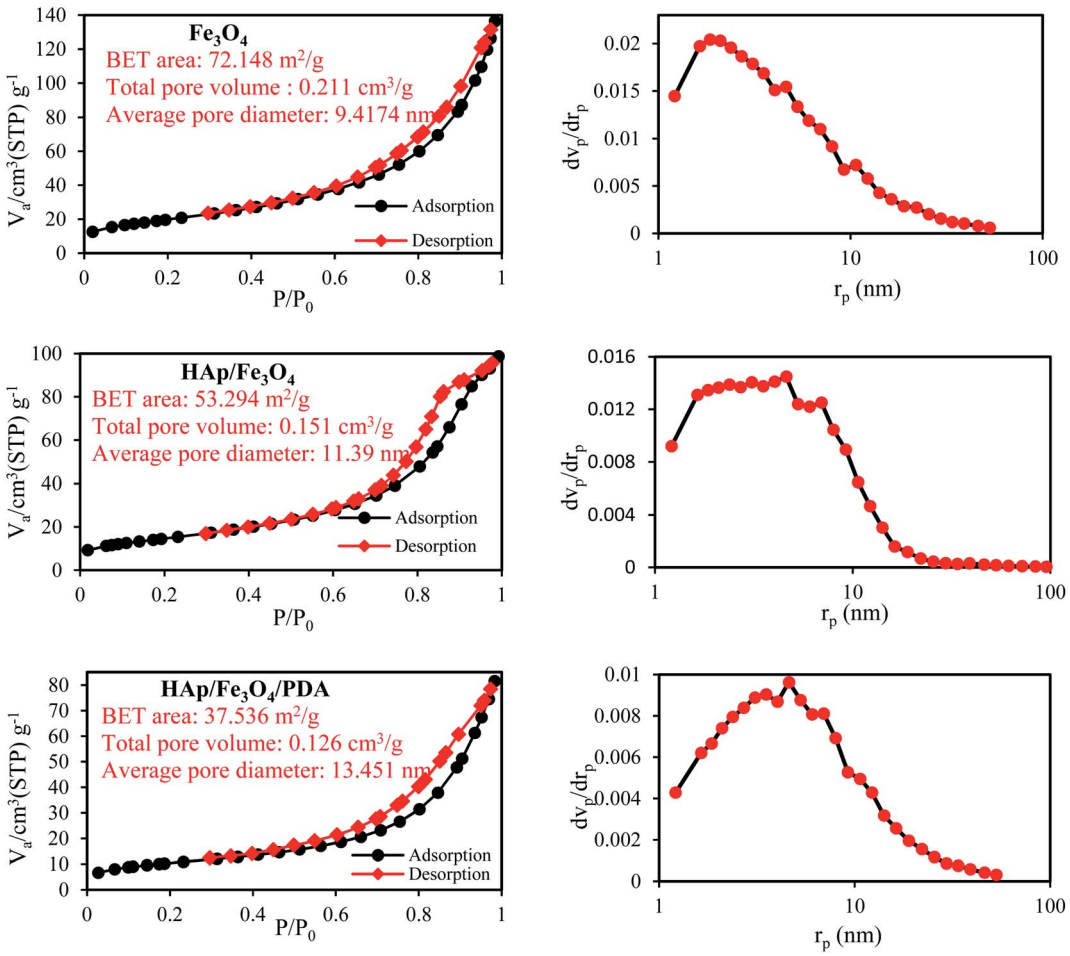

Fig. 2 BET isotherms and BJH pore-size distribution of Fe_3O_4, HAp/Fe_3O_4, and PDA/HAp/Fe_3O_4 samples.

desired magnetic composites, significant changes occur on the HAp surface. Based on the results, the surface roughness of HAp, HAp/Fe_3O_4, and PDA/HAp/Fe_3O_4 samples was measured as 102.693 nm, 65.877 nm, and 65.589 nm, respectively. The reduction in roughness values indicates that Fe_3O_4 nanoparticles and PDA were successfully incorporated on the HAp surface and the desired magnetic composites have been successfully synthesized.

The TEM investigations showed that the produced HAp from chicken bones has a rod shape (Fig. S2b†). According to the results obtained by SEM and XRD investigations, after the addition of Fe_3O_4 magnetic nanoparticles on the HAp surface, the appearance of new particles with different sizes and morphology was observed, indicating the presence of Fe_3O_4 particles on the HAp structure (Fig. S2c†). In the TEM image of PDA/HAp/Fe_3O_4 magnetic composite, the particle aggregation increased which could be due to the formation of polydopamine around the HAp/Fe_3O_4 particles (Fig. S2d†), which is consistent with the SEM results. Particle aggregation and darkness after polydopamine formation around HAp/Fe_3O_4 particles have been attributed to polydopamine formation around particles in some previous studies.[48]

XPS analyses were performed to investigate the chemical composition, PDA/HAp/Fe_3O_4 magnetic composite in the energy range of 0–1300 eV. The acquired findings of XPS test (Fig. 3) revealed that the surface of the material contains only Ca, O, P, N, Fe, and C, which is consistent with the EDX results. More in detail, the peaks at 132.84, 284.21, 347.21, 531.32, 712.06, and 399.87 eV can be corresponded to the binding energies of P 2p, C 1s, Ca 2p, O 1s, Fe 2p, and N 1s, respectively (Fig. 3a).[49] Moreover, the high-energy resolution XPS spectrum of Fe 2p was resolved in two single peaks (Fig. 3b), at 710.68 eV and 723.98 eV respectively, characteristic of Fe $2p_{3/2}$ and Fe $2p_{1/2}$, characteristic of Fe^{3+} (oxide).[50] The high energy resolution spectrum of the N 1s region (Fig. 3c) shows a single peak at 399.87 eV corresponding to the amine groups present in the polydopamine structure, confirming that polydopamine has been successfully incorporated into the magnetic composite structure.[51] The high energy resolution Ca 2p spectrum was fitted with peaks (Fig. 3d) at 346.78 eV and 350.28 eV respectively, characteristic of Ca $2p_{3/2}$ and Ca $2p_{1/2}$ and that can be linked to Ca bonds typical of HAp and to calcium-binding with carbonate due to carbon absorbed from the air. The P 2p spectrum was deconvoluted into peaks at 132.58 eV, 132.78 eV, and 133.48 eV respectively (Fig. 3e), which are justified by the P 2p peaks of phosphate in the HAp structure.[52] The binding energy in the range 525–545 eV was examined to scan the peaks of O 1s (Fig. 3f). As the results show, the O 1s spectrum has peaked in the binding energy range of 529.48 eV, 530.58 eV, and 532.38 eV, which can be categorized into the hydroxyl oxygen (hydroxyl attached to the metal), oxygen absorbed from the surface (water), and network oxygen, which has been confirmed by the literature.[50,53] The peak of C 1s (284.38 eV) in the PDA/HAp/Fe_3O_4 magnetic composite (Fig. 3g) can be linked to C–C or C=C bonds in the polydopamine structure.[54]

Statistical analysis of variance (ANOVA)

The response surface methodology was utilized to reduce the number of tests, to investigate the impact of parameters on the response (% adsorption), and to optimize the effective factors in the adsorption process. This method has enabled researchers to obtain acceptable and sufficient statistical results and information with fewer experiments. In this study, the RSM-CCD method was examined for 5 variables in five levels (Table 1). The results of the experimental and predicted data for the variables are given in Table S1.† Based on the experimental data, the efficiency of the Zn^{2+} ion adsorption process in the desired laboratory conditions is in the range of 62.25% to 98.68%. The second-order polynomial equation of the used CCD method to investigate the appropriate response between the removal efficiency and the critical parameters is described in eqn (4).

$$\text{Zn adsorption} = 97.51 - 0.174X_1 + 11.87X_2 - 3.60X_3 - 1.08X_4 + 13.62X_5 - 0.004X_1X_3 + 0.156X_2X_3 - 2.73X_2X_5 + 0.412X_4X_5 + 0.0007{X_1}^2 - 0.894{X_2}^2 + 0.083{X_3}^2 + 0.017{X_4}^2 \quad (4)$$

According to this equation, the effect of interaction between variables affecting the Zn^{2+} ions adsorption. The effect of parameters with unfavorable interaction (P value > 0.05) was not reported. The findings of model coefficients and analysis of variance (ANOVA) for the Zn^{2+} ions adsorption process using the PDA/HAp/Fe_3O_4 magnetic composite are shown in Table S2.† The importance of each variable on the uptake efficiency is determined based on the values of F and P, and the larger and smaller the values of F and P, respectively, the more important is the effect of the variable on the efficiency of the adsorption process is. Based on the results, the values of F and P for the model were determined as 138.61 and $P < 0.0001$, respectively, showing that the model has very high accuracy and has a confidence level of more than 95% for experimental data.[55] Also, the ANOVA results showed that the interaction between the variables of ultrasonic power/Zn^{2+} concentration, pH/Zn^{2+} concentration, pH/adsorbent dose, and ultrasonic time/adsorbent dose has a vital role in the Zn^{2+} ions removal (according to the values of F and P). In addition to the values of F and P, to assess the capability of the second-order polynomial model, R^2 and Adj-R^2 were used, which were determined as 0.9826 and 0.9755 for the model, respectively. Since the value of parameter R^2 is close to 1, the model has a high ability to describe the adsorption of Zn^{2+} (%) as a function of independent variables,[56] and all variables are effective and important in examining the quadratic polynomial model for the Zn^{2+} ions adsorption.[57] The lack-of-fit value for the Zn^{2+} ions adsorption was determined to be greater than 0.05 using the PDA/HAp/Fe_3O_4 magnetic composite (P-value = 0.4258), which indicates the desirability and good predictability of the model. Based on the lack-of-fit value, the second-order formula has a enough potential to model the interaction between variables.[58] In addition, the low value of CV shows the reliability of the prediction model and shows that the predicted values are slightly different from the experimental data.[59]

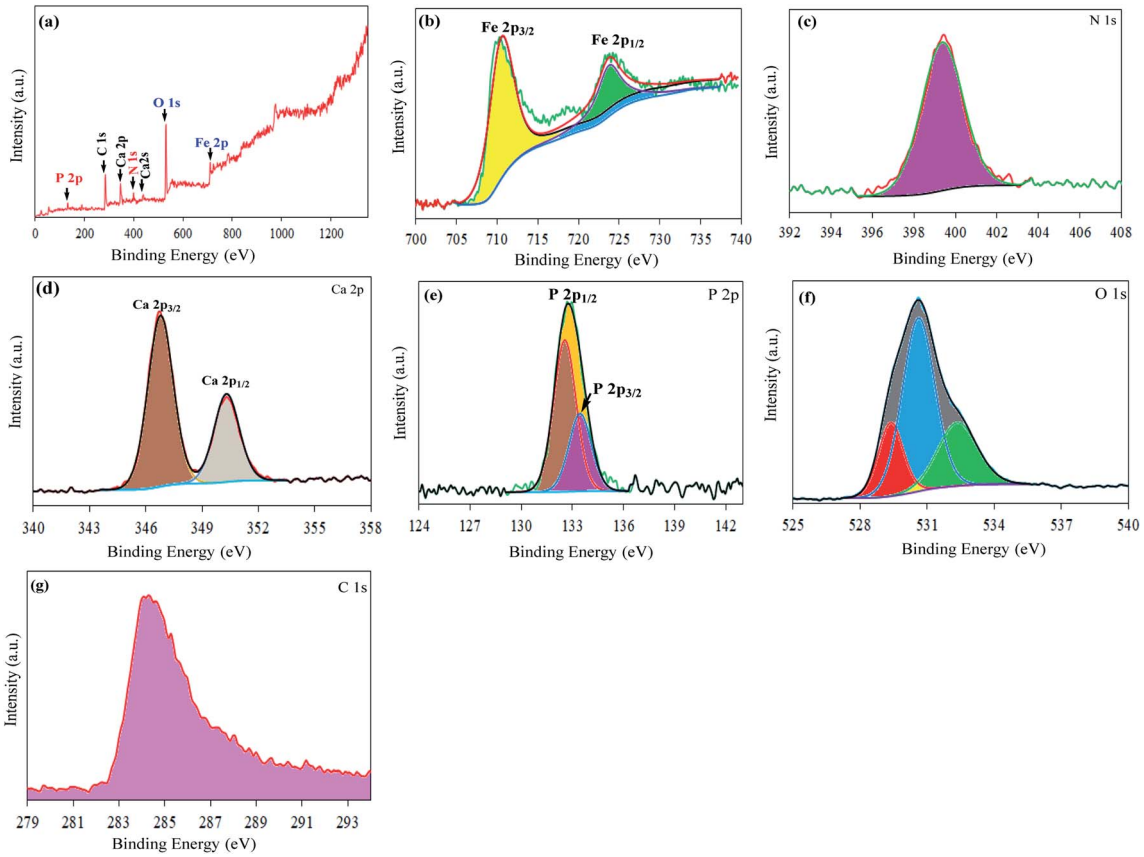

Fig. 3 (a) XPS survey in the range 0–1300 eV and (b–g) the XPS spectra of Fe 2p, N 1s, Ca 2p, P 2p, O 1s, and C 1s of the PDA/HAp/Fe_3O_4 sample.

In the present study, two-dimensional (2D) contour design, three-dimensional (3D) surfaces, and the effect of each variable were coded separately to assess the behavior of variables on the Zn^{2+} ions elimination using the PDA/HAp/Fe_3O_4 magnetic composite (Fig. 4). Based on eqn (4), first-order responses (X_1, X_2, X_3, X_4, and X_5) and two-factor responses (X_1X_3, X_2X_3, X_2X_5, X_4X_5) have positive effects on the adsorption efficiency of Zn^{2+} ions, while other two-factor responses have negative effects on the decontamination process. Therefore, showing the effect of two-factor responses that had negative effects on the adsorption process has been omitted, and 3D levels are shown only for two-factor responses that have had positive effects.

Ultrasonic power was tested in the conditions of 100–300 W and 35 kHz and the results showed that with increasing ultrasonic power, process efficiency increased. Increasing the zinc decontamination by increasing the ultrasonic power can be justified by the collision of Zn^{2+} ions with the composite surface, creating active sites on the adsorbent surface and strengthening the bond between the adsorbate and the solid surface. Same findings have been reported in previous studies, and it has been shown that with increasing ultrasonic power, process efficiency has increased.[60,61]

Based on the results given in Fig. 4, with increasing the contact time, the zinc adsorption increased. This can be justified by sufficient time to absorb zinc.[62]

By determining an optimal pH, it is possible to minimize the hydrolysis of the metal ion or cause the formation of stable complexes of the metal ion with the adsorbent surface.[63] Investigation of the pH effect on the Zn^{2+} ions adsorption showed that by increasing pH in the range of 2 to 6, the process efficiency growth, which could be due to the reduction of competition between H_3O^+ ion and zinc ions in water to occupy active sites. Attaining the low decontamination at acidic pH can also be due to the protonation of functional groups at the adsorbent surface, mainly amine and hydroxyl groups, thus preventing the adsorption of Zn^{2+} ions due to the repulsive electrostatic forces, and finally reducing the uptake efficiency.[64]

As the results show, by increasing the Zn^{2+} ions, the decontamination, and the performance of the PDA/HAp/Fe_3O_4 magnetic composite decreased. The high adsorption efficiency at the low initial concentrations of Zn^{2+} ions can be linked to the accessibility of surface area for the metal ions, while at high concentrations the adsorption efficiency reduces because the active sites are saturated rapidly causing a repulsive electrostatic force between the located metal ions on the composite surface and water.

As the 2D contour design and 3D surfaces have shown, by increasing the composite mass, the removal Zn^{2+} ions from the water is increased, which can be corresponded to the provision of sufficient levels of unsaturated sites to adsorb Zn^{2+} ions. Therefore, according to the obtained findings, the maximum decontamination was obtained at the adsorbate content of 10 mg L^{-1} and the composite mass of 1.2 g L^{-1}.

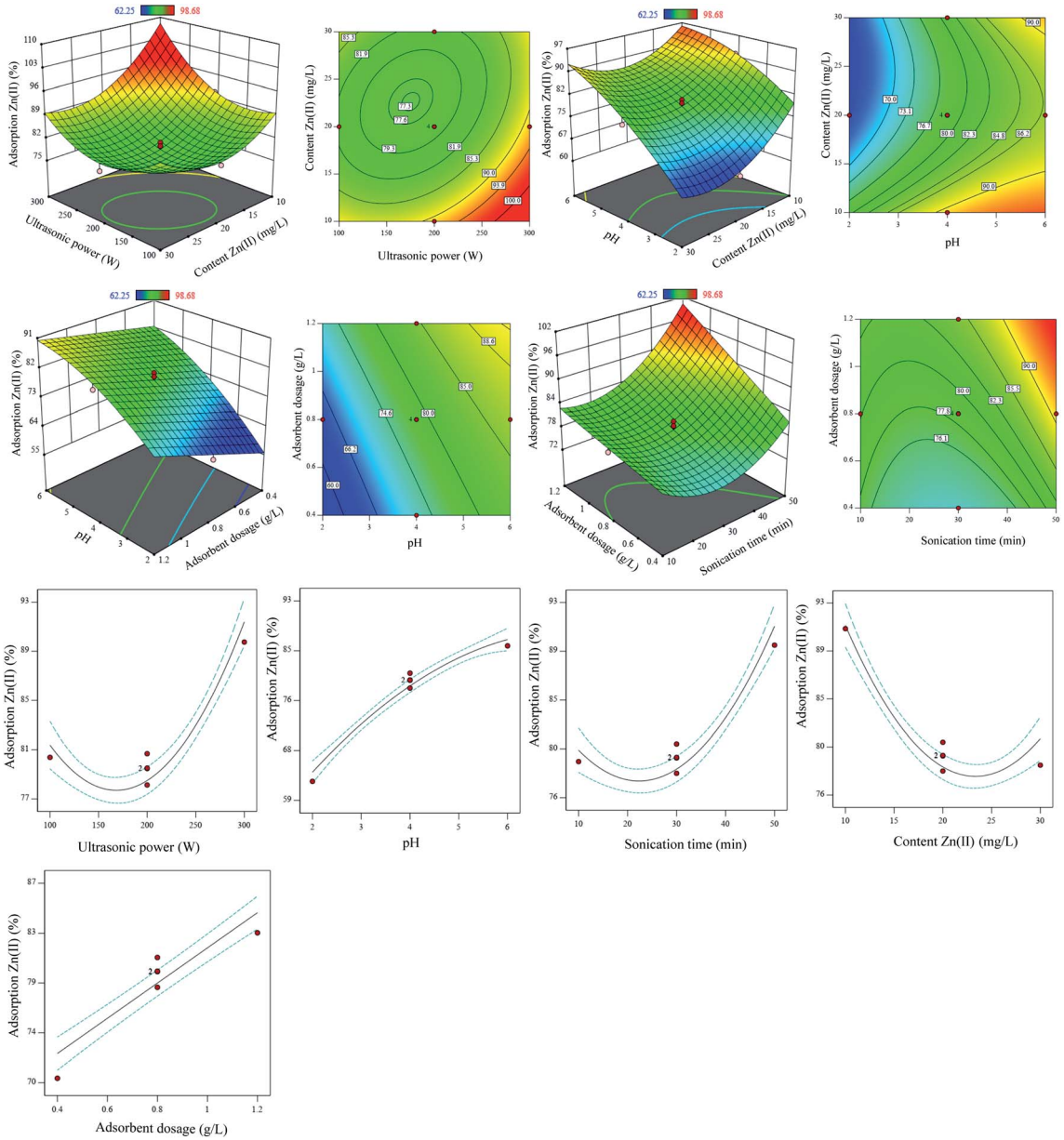

Fig. 4 2D contour design, 3D surfaces, and the effect of one-dimensional variables on the removal efficiency of Zn^{2+} using PDA/HAp/Fe_3O_4 magnetic composite.

Kinetic studies

The kinetic models of pseudo-first-order (PFO), pseudo-second-order (PSO), Elovich, and intraparticle diffusion have been used (eqn (5)–(7)).

PEO:

$$q_t = q_e(1 - e^{-k_1 t}) \quad (5)$$

PSO:

$$q_t = \frac{k_2 q_e^2 t}{1 + k_2 q_e t} \quad (6)$$

Elovich:

$$q_t = \frac{1}{\beta}\ln(1 + \alpha\beta t) \quad (7)$$

Intra diffusion particle:

$$q_t = K_{int}\sqrt{t} + I \quad (8)$$

where, q_t and q_e are the adsorption capacity of Zn^{2+} per gram of dry adsorbent (mg g^{-1}), k_1 constant adsorption rate (min^{-1}), k_2 constant quasi-quadratic kinetic model rate (g mg^{-1} min^{-1}), α is the initial absorbance (mg g^{-1} min^{-1}), β is the desorption constant (g mg^{-1}), I is corresponded to the effects of the boundary layer, and k_i is the constant rate of intraparticle diffusion.

Fig. S3† shows the nonlinear relationship of kinetic models for the Zn^{2+} elimination using PDA/HAp/Fe_3O_4, HAp/Fe_3O_4, and HAp. The constants and variables obtained from the kinetic studies are listed in Table 2. The experimental data of the Zn^{2+} ions removal using the designed adsorbent follows the PSO kinetic model due to the higher correlation coefficient. In addition, the determined value of $q_{e.cal}$ for the PSO is higher than the calculated value of $q_{e.cal}$ using the PFO model and has little difference with $q_{e.exp}$. The experimental data follows PSO, and this shows that chemical reactions are also effective in the Zn^{2+} ions adsorption.[65] The value of the determined α parameter showed that the magnetic composite PDA/HAp/Fe_3O_4 has a greater tendency to adsorb Zn^{2+} ions compared to other adsorbents.

To further investigate the kinetic behavior of zinc ion adsorption by the studied adsorbents, the intraparticle diffusion model was used. This model has the ability to determine the effective mechanisms and controlling stages in the adsorption process. Fig. S4† shows the linear regression of the intraparticle diffusion model for the Zn^{2+} adsorption process using adsorbents produced from hydroxyapatite. In the intraparticle diffusion model, if the value of $I = 0$ (intercept), the adsorption process is mainly controlled by the intraparticle diffusion mechanism. If $I \neq 0$, the internal and external intrusion of particles dominates the whole process.[66] As the results show, for the adsorption of Zn^{2+} using the adsorbents, the value of 'I' was determined $\neq 0$, which indicates that in the Zn^{2+} adsorption, the internal and external diffusion of particles are effective. The adsorption process of Zn^{2+} using the desired adsorbents from the aqueous solution is divided into two stages, the first stage is faster than the second one (see Fig. S4†). The first stage of the adsorption process is due to the adsorption of Zn^{2+} on the adsorbent surface and the second stage is a gradual adsorption step due to the adsorption of Zn^{2+} ions in the adsorbent layers.[19] According to the data in Table 3, the value of I for Zn^{2+} adsorption using PDA/HAp/Fe_3O_4 is higher compared to other adsorbents, which indicates that the limiting phase for Zn^{2+} adsorption using PDA/HAp/Fe_3O_4 has a greater contribution.[67]

Table 2 Parameters of kinetic models for the Zn^{2+} ions adsorption

	Adsorbent		
Kinetic model	HAp	HAp/Fe_3O_4	HAp/Fe_3O_4/PDA
Pseudo-first order			
$q_{e.cal}$	7.835	7.983	8.113
K_{P1st}	0.1247	0.218	0.2441
R^2	0.9074	0.9411	0.9104
RMSE	0.4195	0.2203	0.2442
Pseudo-second order			
$q_{e.cal}$	8.906	8.646	8.71
K_{P2st}	0.01964	0.04389	0.05168
$q_{e.exp}$	7.947	8.151	8.285
R^2	0.954	0.9905	0.9914
RMSE	0.2958	0.0884	0.0757
Elovich equation			
α (mg g^{-1} min)	5.416	84.33	218
β (g mg^{-1})	0.6331	0.9997	1.11
R^2	0.9308	0.8877	0.8933
RMSE	0.3626	0.3043	0.2677

Isotherm studies

In the current study, the nature of Zn^{2+} metal ions adsorption using PDA/HAp/Fe_3O_4 magnetic composite, HAp/Fe_3O_4 magnetic composite, and HAp employing Langmuir, Freundlich, and Dubinin–Radeskovich (DR) isotherm models were evaluated.[68] The desired figures and the determined parameters using the isotherm models are illustrated in Fig. S5† and Table 4, respectively. The experimental data of the Zn^{2+} adsorption process using magnetic composite (PDA/HAp/Fe_3O_4 and HAp/Fe_3O_4) and HAp follow the Freundlich and Langmuir isotherm, respectively. The maximum adsorption capacity (q_m) using PDA/HAp/Fe_3O_4 magnetic composite, HAp/Fe_3O_4 magnetic composite, and HAp was determined as 46.37 mg g^{-1}, 40.07 mg g^{-1}, and 37.57 mg g^{-1}, respectively. The amendment of HAp using Fe_3O_4 nanoparticles and PDA has increased the adsorption capacity, which is in line with the experimental findings. In addition, according to Table S3,† the adsorption capacity of the adsorbents in this study has a good rank compared to the adsorbents studied for the removal of zinc metal. The amount of adsorption energy (K_L) for the Zn^{2+} ions adsorption process using PDA/HAp/Fe_3O_4 magnetic composite, HAp/Fe_3O_4 magnetic composite, and HAp was determined as 0.3687 L mg^{-1}, 0.5537 L mg^{-1}, and 0.5746 L mg^{-1}, respectively. The PDA/HAp/Fe_3O_4 magnetic composite has higher adsorption energy compared to others. Also, the zinc adsorption was desirable as the R_L values were calculated in the range of 0–1. The value of the n parameter determined by the Freundlich model for the Zn^{2+} ions adsorption process by all adsorbents was computed >1, thus, the zinc elimination process is physical. Also, the K_f value for the adsorption process using HAp/Fe_3O_4/PDA magnetic composite is higher compared to other adsorbents, which indicates that the adsorption bond created between Zn^{2+} ions and the surface of PDA/HAp/Fe_3O_4 magnetic composite powder is higher and stronger compared to others.[69] The mean value of average energy (E) for the decontamination process using all the composites/adsorbents was determined less than 8 kJ mol^{-1}, which re-affirms the physical nature of the zinc removal,[70] as well as the A_T and b_T parameters showing that the interactions between the composites/adsorbent surface and

Table 3 Constants and variables determined for the intraparticle diffusion model

	Adsorbent		
Intraparticle diffusion	HAp	HAp/Fe_3O_4	HAp/Fe_3O_4/PDA
$K_{i,1}$ (mg g^{-1} $min^{-1/2}$)	1.1262	0.8264	0.745
I_1 (mg g^{-1})	1.8558	3.9887	4.5379
R^2	0.9847	0.9388	0.9551
$K_{i,2}$ (mg g^{-1} $min^{-1/2}$)	0.1013	0.0514	0.0386
I_2 (mg g^{-1})	7.1991	7.7661	7.9992
R^2	0.8311	0.8324	0.84

Table 4 Variables of isotherms for Zn^{2+} ions adsorption process using the produced adsorbents

Models	Parameters	Adsorbent		
		HAp	HAp/Fe_3O_4	HAp/Fe_3O_4/PDA
Langmuir	q_m (mg g^{-1})	37.57	40.07	46.37
	K_L (L mg^{-1})	0.3687	0.5537	0.5746
	R^2	0.9583	0.9176	0.8222
	R_L	0.026–0.213	0.017–0.152	0.018–0.157
	RMSE	2.29	3.677	6.531
Freundlich	N	3.534	3.688	3.48
	K_f (mg g^{-1} (L $mg^{-1})^{-1/n}$)	13.21	15.85	18.15
	R^2	0.9509	0.9866	0.9928
	RMSE	2.485	1.482	1.314
Dubinin–Radushkevich (D–R)	E (kJ mol^{-1})	0.995	1.675	1.758
	q_m (mg g^{-1})	31.28	32.57	36.79
	$\beta \times 10^{-7}$ (mol^2 J^{-2})	5.045	1.782	1.618
	R^2	0.8102	0.7029	0.5883
	RMSE	4.885	6.98	9.939
Temkin	b_T (kJ mol^{-1})	0.36	0.372	0.382
	A_T (L g^{-1})	5.266	11.43	27.46
	R^2	0.9831	0.9881	0.9162
	RMSE	1.458	1.397	4.484

Zn^{2+} are weak and, as a consequence, that the adsorption process may be physical.[71]

Effect of foreign ions and reusability of the adsorbent

Industrial wastewater usually has different anions and cations due to the passage of different leachate fields and agricultural lands, which can affect the ability of adsorbents in the decontamination process.[72] Sodium (Na^+), calcium (Ca^{2+}), and magnesium (Mg^{2+}) ions are the common cations existing in water and wastewater,[73] therefore in the present study, the impact of these ions on the Zn adsorption was investigated in the concentration of 0.05–0.5 M (Fig. S6a–c†). Based on the results, by increasing foreign ions molarity, the Zn^{2+} adsorption decreased for all three types of adsorbents. This decrease may be due to the competition of Na^+, Ca^{2+}, and Mg^{2+} with Zn^{2+} for the accessible sites on the adsorbent. As a result, the zinc decontamination process has decreased.

One of the influential factors in reducing the operative costs of the adsorption method is the adsorbent synthesis costs. Reuse of adsorbents, in addition to reducing costs, can also save on the use of primary sources for the generation of adsorbents. For this purpose, the adsorption/desorption process of Zn^{2+} ion was investigated employing synthesized HAp based adsorbents up to 10 cycles (Fig. S6b†). After each cycle, the adsorbent was properly regenerated, as described in Section 2.4. The acquired findings revealed that with elevating the number of adsorption/desorption steps, the ability of adsorbents to remove Zn^{2+} ions decreased. Decreasing the adsorption efficiency by increasing the stages of adsorption/desorption can be linked to various factors like damage and/or modification of the structure, as well as adsorbent sites saturation.[74]

Mechanism of Zn^{2+} adsorption process

To describe the adsorption of metal ions from aqueous solution using hydroxyapatite adsorbents (HAP) various possible mechanisms such as ion exchange, decomposition–deposition, and formation of surface complexes have been suggested. Recently, the decomposition–deposition mechanism has received much attention from researchers. The possible mechanism of this process is described as follows:

Dissolution:

$$Ca_{10}(PO_4)_6(OH)_2 + 14H^+ \rightarrow 10Ca^{2+} + 6H_2PO_4^- + 2H_2O \quad (9)$$

Precipitation:

$$10M^{2+} + 6H_2PO_4^- + 2H_2O \rightarrow 14H^+ + M_{10}(PO_4)_6(OH)_2 \quad (10)$$

It is assumed that the mechanism of Zn^{2+} adsorption using PDA/HAp/Fe_3O_4 nanocomposite has three steps: (1) diffusion of metal ions (M^{2+}) from the aqueous solution to the surface of the calcium hydroxyapatite matrix; (2) adsorption of Zn^{2+} ions to the adsorptive sites; and (3) replacement of Zn^{2+} with Ca^{2+} in hydroxyapatite.[26]

In addition to hydroxyapatite, Fe_3O_4 nanoparticles can also be effective in the adsorption of Zn^{2+}, the process schematic of which is shown in Fig. 5. In aqueous systems, the surface of iron oxide is covered with FeOH groups. The hydroxyl group present on the surface of iron nanoparticles can have negative (FeO^-) and positive ($FeOH_2^+$) charges at pHs above or below pH_{ZPC}, respectively. Iron nanoparticles contain Fe^{2+} which can be hydrolyzed at different pHs to form $FeOH^+$, $Fe(OH)_2^\circ$, and $Fe(OH)_3^-$. Thus, an electrostatic absorption force is created between the ionic species of the metal Zn^{2+} and the surface of the iron nanoparticles. In previous studies, the pH_{ZPC} of Fe_3O_4 nanoparticles has been reported to be 7.4, which is almost neutral.[26] According to Fig. 5, with increasing the initial pH, the adsorption efficiency of Zn^{2+} using PDA/HAp/Fe_3O_4 increased. It shows the driving force increased between the adsorbent surface and the Zn^{2+} ion. As the pH increases, the surface

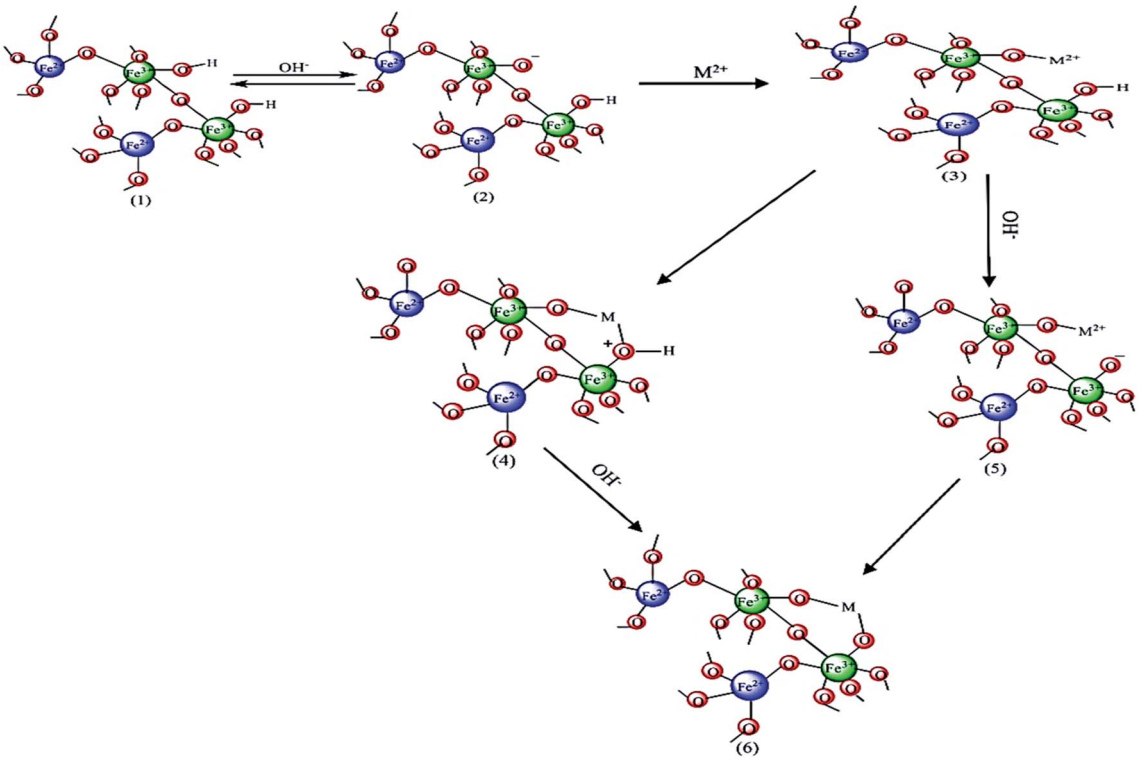

Fig. 5 Schematic of Zn^{2+} (M^{2+}) adsorption process using Fe_3O_4 nanoparticles in PDA/HAp/Fe_3O_4 nanocomposite.

charges of $FeOH_2^+$ in the composite are converted to FeO^- and the electrostatic attraction between Zn^{2+} and FeO^- increases (Fig. 5).

PDA/HAp/Fe_3O_4 also contains polydopamine, which can affect the adsorption process. In the structure of polydopamine, there are –OH and NH groups that can be converted to different states at different pHs. The different forms of the –OH group in the polydopamine are similar to the functional group in the iron oxide nanoparticles, which affects the adsorption of Zn^{2+}. In general, it can be mentioned that the process of adsorption of metal ions with PDA is happened through chelation and coordination.[75] The interaction between PDA and Zn^{2+} ions is depicted in Fig. 6.

Conclusions

Modification of raw minerals can increase their adsorption capacity and performance in the adsorption process. Herein, HAp generated from chicken bones was modified using Fe_3O_4 nanoparticles and PDA and used as a promising composite to decontaminate Zn^{2+} from a liquid media. The surface and structural characteristics of the composites were explored by

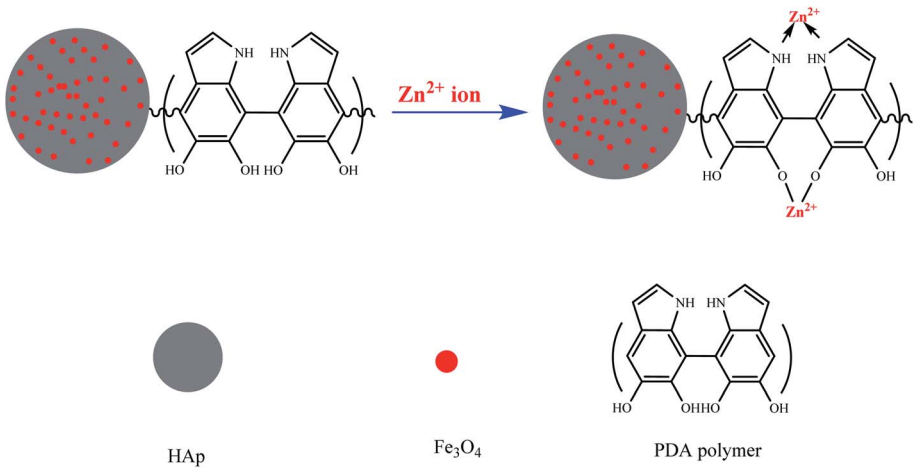

Fig. 6 Schematic of Zn^{2+} adsorption using PDA in PDA/HAp/Fe_3O_4 nanocomposite structure.

various techniques, which showed that Fe_3O_4 nanoparticles and PDA have been successfully placed in the HAp structure and have good interaction with each other. The magnetic saturation value for Fe_3O_4, HAp/Fe_3O_4 magnetic composite, and PDA/HAp/Fe_3O_4 magnetic composite was 84.283 emu g^{-1}, 30.305 emu g^{-1}, and 24.014 emu g^{-1}, respectively, which depicted that the composites are easily separated from the aqueous solution and can be reused. RSM-CCD was used to study the effect of operative parameters on the removal efficiency and also the interaction between them. The results of ANOVA revealed that the model has a good potential to evaluate the interaction between the parameters on the decontamination efficiency of Zn^{2+} ions. The results showed that the equilibrium and kinetic behavior follow the Freundlich and pseudo-second-order models, respectively. The *n* and *E* factors showed that the zinc adsorption is physical and desirable. Adsorption/desorption capacity of PDA/HAp/Fe_3O_4 magnetic composite showed that by elevating the adsorption/desorption stages, the ability and performance of the adsorbent decreases. Therefore, based on the surface and structural properties, the performance and adsorption ability of Zn^{2+} ions, PDA/HAp/Fe_3O_4 magnetic composite can be suggested as a promising composite for the zinc ions removal from water matrixes.

Author contributions

R. Foroutan: formal analysis, methodology. S. J. Peighambardoust: funding acquisition, methodology. S. Hemmati: methodology, conceptualization, A. Ahmadi: writing – original draft. E. Falletta: writing – review& editing, methodology. B. Ramavandi: supervision, conceptualization, writing – review& editing. C. L. Bianchi: supervision, conceptualization.

Conflicts of interest

There are no conflicts to declare.

Acknowledgements

The authors thank to the Bushehr University of Medical Sciences, Iran for technical supports to conduct this work. This research was undertaken, in part, thanks to funding from Velux Stiftung Foundation through the project 1381 SUNFLOAT–Water decontamination by sunlight-driven floating photocatalytic systems.

References

1 P. Wei, H. Lou, X. Xu, W. Xu, H. Yang, W. Zhang and Y. Zhang, *Appl. Surf. Sci.*, 2021, **539**, 148195.
2 H. Zhao and Y. Li, *J. Environ. Chem. Eng.*, 2021, **9**, 105316.
3 M. Chen, R. Bi, R. Zhang, F. Yang and F. Chen, *Colloids Surf., A*, 2021, **617**, 126384.
4 Q. U. Ain, H. Zhang, M. Yaseen, U. Rasheed, K. Liu, S. Subhan and Z. Tong, *J. Cleaner Prod.*, 2020, **247**, 119088.
5 J. Ma, H. Wang, D. Li, L. Liu and H. Yang, *Colloids Surf., A*, 2021, **616**, 126324.
6 R. Gayathri, K. P. Gopinath and P. S. Kumar, *Chemosphere*, 2021, **262**, 128031.
7 X. Song, Y. Cao, X. Bu and X. Luo, *Appl. Surf. Sci.*, 2021, **536**, 147958.
8 M. T. H. Siddiqui, H. A. Baloch, S. Nizamuddin, N. M. Mubarak, S. A. Mazari, G. J. Griffin and M. Srinivasan, *Renewable Energy*, 2021, **172**, 1103–1119.
9 A. Pooladi and R. Bazargan-Lari, *J. Mater. Res. Technol.*, 2020, **9**, 14841–14852.
10 F. Foroughi, S. A. Hassanzadeh-Tabrizi, J. Amighian and A. Saffar-Teluri, *Ceram. Int.*, 2015, **41**, 6844–6850.
11 L. Luan, B. Tang, S. Ma, L. Sun, W. Xu, A. Wang and Y. Niu, *J. Mol. Liq.*, 2021, **330**, 115634.
12 S. Meski, H. Khireddine, S. Ziani, S. Rengaraj and M. Sillanpää, *Desalin. Water Treat.*, 2010, **16**, 271–281.
13 R. Shahrokhi-Shahraki, C. Benally, M. G. El-Din and J. Park, *Chemosphere*, 2021, **264**, 128455.
14 A. Ahmadi, R. Foroutan, H. Esmaeili and S. Tamjidi, *Environ. Sci. Pollut. Res.*, 2020, 1–14.
15 K. Sangeetha, G. Vidhya, G. Vasugi and E. K. Girija, *J. Environ. Chem. Eng.*, 2018, **6**, 1118–1126.
16 T. Sheela, Y. A. Nayaka, R. Viswanatha, S. Basavanna and T. G. Venkatesha, *Powder Technol.*, 2012, **217**, 163–170.
17 R. Foroutan, A. Oujifard, F. Papari and H. Esmaeili, *3 Biotech*, 2019, **9**, 78.
18 Z. Bonyadi, P. S. Kumar, R. Foroutan, R. Kafaei, H. Arfaeinia, S. Farjadfard and B. Ramavandi, *Korean J. Chem. Eng.*, 2019, **36**, 1595–1603.
19 R. Foroutan, R. Mohammadi, S. J. Peighambardoust, S. Jalali and B. Ramavandi, *Environ. Technol. Innovation*, 2020, **19**, 101031.
20 Z. Khademi, B. Ramavandi and M. T. Ghaneian, *J. Environ. Chem. Eng.*, 2015, **3**, 2057–2067.
21 R. Foroutan, H. Esmaeili, S. D. Rishehri, F. Sadeghzadeh, S. Mirahmadi, M. Kosarifard and B. Ramavandi, *Data Br.*, 2017, **12**, 485–492.
22 R. Asadi, H. Abdollahi, M. Gharabaghi and Z. Boroumand, *Adv. Powder Technol.*, 2020, **31**, 1480–1489.
23 A. M. Ahmed, M. I. Ayad, M. A. Eledkawy, M. A. Darweesh and E. M. Elmelegy, *Heliyon*, 2021, **7**, e06315.
24 M. Ferri, S. Campisi, M. Scavini, C. Evangelisti, P. Carniti and A. Gervasini, *Appl. Surf. Sci.*, 2019, **475**, 397–409.
25 I. Mobasherpour, E. Salahi and M. Pazouki, *Arabian J. Chem.*, 2012, **5**, 439–446.
26 R. Foroutan, S. J. Peighambardoust, S. S. Hosseini, A. Akbari and B. Ramavandi, *J. Hazard. Mater.*, 2021, **413**, 125428.
27 K.-W. Jung, S. Y. Lee, J.-W. Choi and Y. J. Lee, *Chem. Eng. J.*, 2019, **369**, 529–541.
28 P. Sirajudheen, P. Karthikeyan, S. Vigneshwaran and S. Meenakshi, *Int. J. Biol. Macromol.*, 2021, **175**, 361–371.
29 Y. Kim, E. Coy, H. Kim, R. Mrówczyński, P. Torruella, D.-W. Jeong, K. S. Choi, J. H. Jang, M. Y. Song, D.-J. Jang, F. Peiro, S. Jurga and H. J. Kim, *Appl. Catal., B*, 2021, **280**, 119423.
30 W.-Z. Qiu, H.-C. Yang and Z.-K. Xu, *Adv. Colloid Interface Sci.*, 2018, **256**, 111–125.

31 Q. Zeng, X. Qi, M. Zhang, X. Tong, N. Jiang, W. Pan, W. Xiong, Y. Li, J. Xu, J. Shen and L. Xu, *Int. J. Biol. Macromol.*, 2020, **145**, 1049–1058.
32 A. Q. Alorabi, M. Shamshi Hassan and M. Azizi, *Arabian J. Chem.*, 2020, **13**, 8080–8091.
33 R. Foroutan, S. J. Peighambardoust, H. Aghdasinia, R. Mohammadi and B. Ramavandi, *Environ. Sci. Pollut. Res.*, 2020, **27**, 44218–44229.
34 R. Foroutan, M. Ahmadlouydarab, B. Ramavandi and R. Mohammadi, *J. Environ. Chem. Eng.*, 2018, **6**, 6049–6058.
35 H. M. Khan, T. Iqbal, C. H. Ali, S. Yasin and F. Jamil, *Renewable Energy*, 2020, **154**, 1035–1043.
36 M. Zendehdel, B. Shoshtari-Yeganeh, H. Khanmohamadi and G. Cruciani, *Process Saf. Environ. Prot.*, 2017, **109**, 172–191.
37 Q. U. Ain, U. Rasheed, M. Yaseen, H. Zhang and Z. Tong, *J. Hazard. Mater.*, 2020, **397**, 122758.
38 M. Mousavi and A. Habibi-Yangjeh, *Adv. Powder Technol.*, 2018, **29**, 94–105.
39 I. Dayana, T. Sembiring, A. P. Tetuko, K. Sembiring, N. Maulida, Z. Cahyarani, E. A. Setiadi, N. S. Asri, M. Ginting and P. Sebayang, *J. Mol. Liq.*, 2019, **294**, 111557.
40 A. Mohammadi, H. Daemi and M. Barikani, *Int. J. Biol. Macromol.*, 2014, **69**, 447–455.
41 C. Miao, L. Yang, Z. Wang, W. Luo, H. Li, P. Lv and Z. Yuan, *Fuel*, 2018, **224**, 774–782.
42 K. C. Vinoth Kumar, T. Jani Subha, K. G. Ahila, B. Ravindran, S. W. Chang, A. H. Mahmoud, O. B. Mohammed and M. A. Rathi, *Saudi J. Biol. Sci.*, 2021, **28**, 840–846.
43 X. Lei, T. Xu, W. Yao, Q. Wu and R. Zou, *J. Taiwan Inst. Chem. Eng.*, 2020, **106**, 148–158.
44 D. O. Obada, E. T. Dauda, J. K. Abifarin, D. Dodoo-Arhin and N. D. Bansod, *Mater. Chem. Phys.*, 2020, **239**, 122099.
45 F. Kermani, S. Mollazadeh, S. Kargozar and J. Vahdati Khakhi, *Mater. Sci. Eng. C*, 2021, **118**, 111533.
46 Q. Wu, M. S. Siddique and W. Yu, *J. Hazard. Mater.*, 2021, **401**, 123261.
47 A. Savari, S. Hashemi, H. Arfaeinia, S. Dobaradaran, R. Foroutan, A. H. Mahvi, M. Fouladvand, G. A. Sorial, S. Farjadfard and B. Ramavandi, *Adv. Powder Technol.*, 2020, **31**, 3521–3532.
48 S. Hu, J. Wu, Z. Cui, J. Si, Q. Wang and X. Peng, *J. Appl. Polym. Sci.*, 2020, **137**, 49077.
49 Y. Pang, L. Kong, D. Chen, G. Yuvaraja and S. Mehmood, *J. Hazard. Mater.*, 2020, **384**, 121447.
50 Y.-Y. Wu, Y. Teng, M. Zhang, Z.-P. Deng, Y.-M. Xu, L.-H. Huo and S. Gao, *Sens. Actuators, B*, 2021, **329**, 129126.
51 L. Cheng, H. Wu, J. Li, H. Zhao and L. Wang, *Corros. Sci.*, 2021, **178**, 109064.
52 S. Dhatchayani, S. Vijayakumar, N. Sarala, B. Vaseeharan and K. Sankaranarayanan, *J. Drug Delivery Sci. Technol.*, 2020, **60**, 101963.
53 M. Gao, W. Wang, H. Yang and B.-C. Ye, *Microporous Mesoporous Mater.*, 2019, **289**, 109620.
54 B. Moreno-Perez, Z. Matamoros-Veloza, J. C. Rendon-Angeles, K. Yanagisawa, A. Onda, J. E. Pérez-Terrazas, E. E. Mejia-Martínez, O. Burciaga Díaz and M. Rodríguez-Reyes, *Bol. Soc. Esp. Ceram. Vidrio*, 2020, **59**, 50–64.
55 R. Foroutan, S. J. Peighambardoust, R. Mohammadi, B. Ramavandi and D. C. Boffito, *Environ. Technol. Innovation*, 2021, **21**, 101250.
56 U. K. Garg, M. P. Kaur, V. K. Garg and D. Sud, *Bioresour. Technol.*, 2008, **99**, 1325–1331.
57 R. Foroutan, R. Mohammadi and B. Ramavandi, *Fuel*, 2021, **291**, 120151.
58 S. Rahdar, K. Pal, L. Mohammadi, A. Rahdar, Y. Goharniya, S. Samani and G. Z. Kyzas, *J. Mol. Struct.*, 2021, **1231**, 129686.
59 E. Cheraghipour and M. Pakshir, *J. Environ. Chem. Eng.*, 2021, **9**, 104883.
60 P. Wang, W. Ji, M. Li, G. Zhang and J. Wang, *Ultrason. Sonochem.*, 2017, **38**, 289–297.
61 C. Liu, Y. Sun, D. Wang, Z. Sun, M. Chen, Z. Zhou and W. Chen, *Ultrason. Sonochem.*, 2017, **34**, 142–153.
62 F. Bahador, R. Foroutan, H. Esmaeili and B. Ramavandi, *Carbohydr. Polym.*, 2021, **251**, 117085.
63 B. M. Córdova, T. Venâncio, M. Olivera, R. G. Huamani-Palomino and A. C. Valderrama, *Int. J. Biol. Macromol.*, 2021, **169**, 130–142.
64 D. Gan, Q. Huang, J. Dou, H. Huang, J. Chen, M. Liu, Y. Wen, Z. Yang, X. Zhang and Y. Wei, *Appl. Surf. Sci.*, 2020, **504**, 144603.
65 H. Xu, X. Hu, Y. Chen, Y. Li, R. Zhang, C. Tang and X. Hu, *Colloids Surf., A*, 2021, **612**, 126005.
66 W. Wang, M. Gao, M. Cao, J. Dan and H. Yang, *Sci. Total Environ.*, 2021, **759**, 143542.
67 R. Foroutan, R. Mohammadi, A. Ahmadi, G. Bikhabar, F. Babaei and B. Ramavandi, *Chemosphere*, 2022, **286**, 131632.
68 S. Pashaei-Fakhri, S. J. Peighambardoust, R. Foroutan, N. Arsalani and B. Ramavandi, *Chemosphere*, 2021, **270**, 129419.
69 C. Wang, X. Jiang, L. Zhou, G. Xia, Z. Chen, M. Duan and X. Jiang, *Chem. Eng. J.*, 2013, **219**, 469–477.
70 S. O. Alaswad, K. B. Lakshmi, P. N. Sudha, T. Gomathi and P. Arunachalam, *Int. J. Biol. Macromol.*, 2020, **164**, 1809–1824.
71 E. Binaeian, S. Babaee Zadvarzi and D. Yuan, *Int. J. Biol. Macromol.*, 2020, **162**, 150–162.
72 Q. Zhou, Y. Lin, X. Li, C. Yang, Z. Han, G. Zeng, L. Lu and S. He, *Bioresour. Technol.*, 2018, **249**, 457–463.
73 X. Li, C. Yang, G. Zeng, S. Wu, Y. Lin, Q. Zhou, W. Lou, C. Du, L. Nie and Y. Zhong, *Algal Res.*, 2020, **46**, 101804.
74 R. Foroutan, R. Mohammadi, F. MousaKhanloo, S. Sahebi, B. Ramavandi, P. S. Kumar and K. H. Vardhan, *Adv. Powder Technol.*, 2020, **31**, 3993–4004.
75 S. Zhang, Y. Zhang, G. Bi, J. Liu, Z. Wang, Q. Xu, H. Xu and X. Li, *J. Hazard. Mater.*, 2014, **270**, 27–34.